A cold-atom beam clock based on coherent population trapping

View Online   Export Citation   CrossMark

John D. Elgin,[1,2] Thomas P. Heavner,[1] John Kitching,[1] (iD) Elizabeth A. Donley,[1] (iD) Jayson Denney,[3]
and Evan A. Salim[3,a] (iD)

AFFILIATIONS

[1]Time and Frequency Division, National Institute of Standards and Technology, Boulder, Colorado 80305, USA
[2]Department of Physics, University of Colorado, Boulder, Colorado 80309, USA
[3]ColdQuanta, Inc., 3030 Sterling Cir, Boulder, Colorado 80301, USA

[a]Electronic mail: evan.salim@coldquanta.com

ABSTRACT

We present results from an atomic clock that employs a beam of cold ^{87}Rb atoms and spatially separated (Ramsey) coherent population trapping interrogation of the hyperfine clock transition at 6.834 GHz. The cold atomic beam is generated through the use of a 2D$^+$-magneto-optical trap. The interrogation is performed on the D2 line of ^{87}Rb, and the optical fields use a counter-propagating σ_+–σ_- probing scheme. The use of cold atoms allows for relatively narrow Ramsey fringes even for a small spatial separation between the two interrogation zones (4.6 cm). The resulting clock has a short-term stability of $3 \times 10^{-11}/\sqrt{\tau}$.

An important class of atomic clocks, including commercial cesium frequency standards, employs a thermal beam of atoms directed through two spatially separated microwave cavities to measure the hyperfine clock transition using Ramsey spectroscopy.[1] Most commercial frequency standards utilize this technique, and until the advent of laser-cooled atomic fountains and optical clocks, many national metrology laboratories around the world relied on high-performance Cs beam devices to realize the International System of Units (SI) second.[2] Due to the relatively high velocity of the atoms in the thermal beam and the size of the microwave cavities, there is a strict trade-off between the flight tube length and the resonance linewidth. This precludes the use of such systems as candidates for compact devices.

Recent interest in compact, low power clocks has led to the increased use of coherent population trapping (CPT) using optical fields modulated at microwave frequencies, thus eliminating the need for microwave cavities.[3–5] A clock based on Ramsey spectroscopy obtained using CPT has also been demonstrated with thermal beams.[6,7] In related further work, thermal beams have been used to perform precision stark-shift measurements with CPT,[8] and cold-atom beams have been used to perform Ramsey spectroscopy with stimulated Raman transitions.[9]

Interest in the use of laser cooled atoms for atomic clocks has grown over the last 10 years, including clocks based on direct microwave interrogation,[10] as well as CPT spectroscopy.[11–14] Cold-atom

CPT (CA-CPT) clocks provide many advantages over traditional vapor cell CPT clocks. The performance of vapor cell CPT clocks suffers from long-term frequency instability, due to the high-pressure buffer gases and light shifts. CA-CPT clocks forego the need for a buffer gas and as such eliminate any associated shifts, offering potential performance improvements in terms of accuracy and long-term frequency stability. The use of cold atoms can also provide a means to ameliorate the scaling of atomic-beam CPT clocks and provide a path toward using atomic beams in compact clocks.

Most CPT experiments to date have been performed using D1 interrogation because of the relatively large homogeneous broadening present in buffer-gas vapor cells.[12,15] However, interrogation with the D2 line is attractive because this can greatly reduce the complexity of the laser system in a cold-atom clock as a single laser can be the source for both the cooling beams and the CPT beams. By reducing the complexity of the laser system and eliminating the need for a second laser, the system is an ideal candidate for a compact low-power device.

The most prominent concern with using the D2 line is a reduction of CPT signal contrast due to interference of overlapping lambda systems, caused by the high density of excited states combined with homogeneous broadening from the buffer gas in vapor-cell clocks.[15] By laser cooling Rb, we no longer need buffer gases to enhance the interrogation time, thereby narrowing the transitions and preventing interference between adjacent lambda systems.

Additionally, the high density D2 line states introduce frequency shifts due to the off-resonant coupling to adjacent states or off-resonant light shifts.[16] These shifts are worse for D2 than D1 interrogation because there are more hyperfine excited states present on the D2 transition than the D1, and they are more closely spaced to each other. For portable applications where size and power are significant concerns, increased off-resonant light shifts can be an acceptable trade-off for the reduction in instrument complexity achieved with a single laser.

Here, we combine cold-atom technology and the atomic beam CPT architecture to demonstrate a prototype for a cold atomic beam CPT clock based on D2 interrogation. Single-pulse and Ramsey CPT spectroscopy is demonstrated, and the clock is locked to the central Ramsey fringe at the hyperfine splitting frequency. An early analysis of the frequency stability of the clock is presented, along with a discussion of the main systematic biases that limit the long-term stability. Our use of the cold-atom beam geometry over a 3D magneto-optical trap (MOT) configuration was motivated by the relative simplicity of the optics as well as the expected reduced sensitivity to vacuum impurities.

A schematic diagram of the optical setup is shown in Fig. 1. The experiment uses a single Distributed Bragg reflector (DBR) laser diode at 780 nm, locked to the $F = 2 \rightarrow F' = 1, 3$ crossover transition in ^{87}Rb. A tapered amplifier is used to increase the optical power to overcome the losses of the electro-optic modulators (EOMs) and to enable the use of a single laser for both the laser cooling and the CPT probe light.

The laser cooling light is frequency shifted 15 MHz red from the cycling transition ($F = 2 \rightarrow F' = 3$) by the use of a double-pass acousto-optic modulator (AOM). The light is then passed through a fiber-coupled EOM driven at 6.58 GHz to add sidebands at the repump frequency. Next, the light is directed through a high isolation, kilohertz bandwidth shutter, which is used to pulse the light for the magneto-optical trap (MOT) on and off. Most of the cooling light (~35 mW) is used to create the 2D-MOT in the source section of the vacuum cell, while a portion (~2–3 mW) of the light is picked off and directed along the longitudinal axis of the cold-atoms for the 2D$^+$-MOT configuration.[17]

We have used this benchtop laser system to validate a candidate architecture that we believe lends itself to small-scale integration of a future device: The lower graphic of Fig. 1 shows a possible implementation of the CPT clock laser system in a photonically integrated circuit (PIC). As the CPT beam clock is operated in a pulsed mode, the PIC source can be operated dynamically, where the laser is tuned to an appropriate frequency for laser cooling during the loading of the atom beam and then jumped to the appropriate offset for CPT during the state prep and interrogation period. Frequency agility in the laser is achieved by locking the source to a sideband generated by the leftmost phase modulator in the diagram, where the laser is locked to the ^{85}Rb cooling transition, while repump light and the CPT sidebands are generated with the phase modulator on the right side. Intensity tuning and shuttering is achieved using an in-PIC optical amplifier and switch.
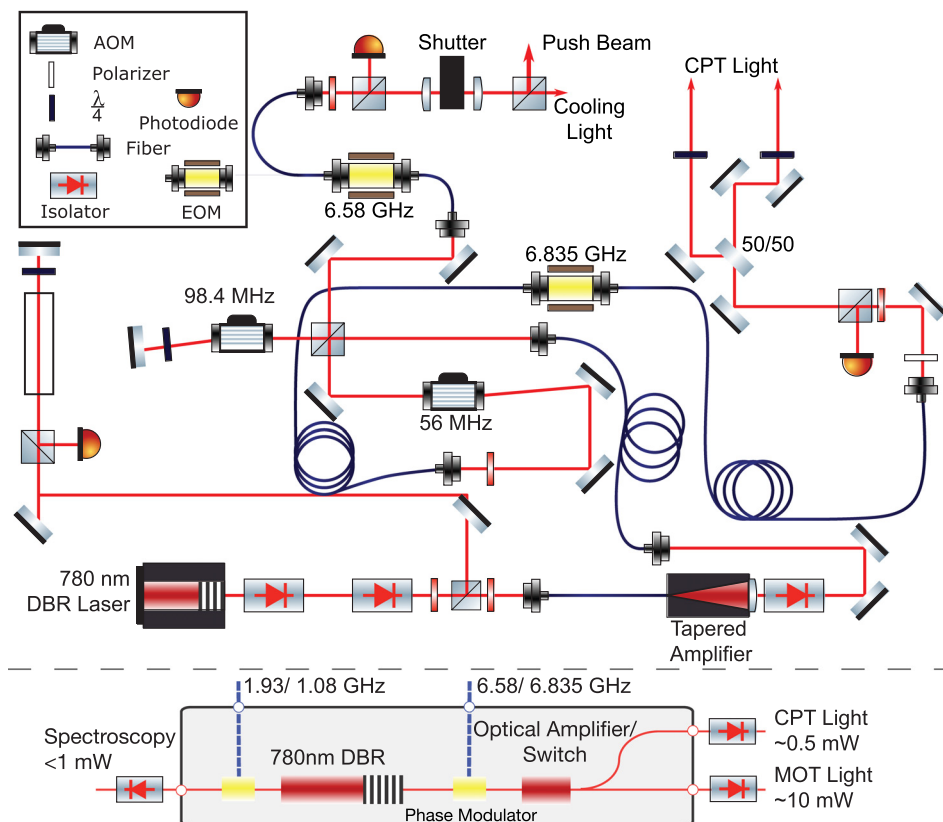

FIG. 1. Illustration of the laser and optical system for the cold-atom beam CPT clock. Both the cooling and CPT light originate from a single laser locked with saturated absorption spectroscopy (SAS). A double-pass acousto-optic modulator (AOM) is used to shift the cooling light to the cycling transition, and another single-pass AOM is used to shift the CPT light to the interrogation transition. Electro-optical modulators are used to add the repump light sidebands (6.58 GHz) to the MOT cooling light and to add 6.835 GHz sidebands for the CPT light. The lower inset shows a possible implementation of the complete laser system into a single photonically integrated circuit.

The light for CPT interrogation of the atoms is picked off, and the frequency is shifted by −56 MHz to bring it into resonance with the CPT transition ($F = 2 \rightarrow F' = 2$, see Fig. 2). The light is then passed through a fiber-coupled EOM driven at 6.835 GHz—the hyperfine splitting frequency of Rb.[18] The carrier and the 1st-order sideband interact with the atomic beam. The microwave power sent to the EOM is adjusted such that the carrier and 1st-order sidebands have nominally the same intensity. The light is then passed through a series of free space optics designed to approximately match the optical path length between each CPT zone so that the atoms experience equal microwave phases in the two zones, thus minimizing the end-to-end phase shift. Both the cooling light and the CPT light make use of intensity servos, which feed back to the amplitudes of the RF driving their respective AOMs.

The clock is operated in the pulsed mode to prevent scattered light from the 2D-MOT and the push beam light from interacting with the atoms during the Ramsey CPT interrogation. In the pulsed mode, the mechanical shutter is open for 11 ms and closed for 22 ms so that the clock operates at a repetition rate of 30 Hz.

Figure 3 shows a schematic diagram of the vacuum system. The atomic beam is generated in the source cell and propagates into the interrogation cell. The two glass cells (each about 2 cm × 2 cm × 5 cm) are connected through a 0.8 mm diameter aperture in a silicon plate that allows the two cells to be differentially pumped by the ion pump attached to the interrogation cell. The two cells are separated along the axis of the atomic beam by a gap of about 12 cm. We estimate that the pressures in the source and interrogation cells are about 5×10^{-8} and 10^{-9} Torr, respectively. The silicon plate at the end of the MOT also serves as the exit for the atomic beam. The silicon is partially reflective, and when the push beam is incident on the silicon, a portion of the light is reflected back to provide some longitudinal cooling of the atoms. In the source cell, a Rb dispenser generates the thermal Rb gas which is cooled into a 2D$^+$-MOT. Permanent magnets (not shown) are utilized to generate the 2D anti-Helmholtz field necessary for the MOT.

Inside the interrogation cell is an in-vacuum reflecting optical element, which consists of two highly reflective coated dielectric mirrors arranged in a configuration of a roof mirror. The retroreflector is 11 mm from the centerline of the atomic beam, a distance necessary to
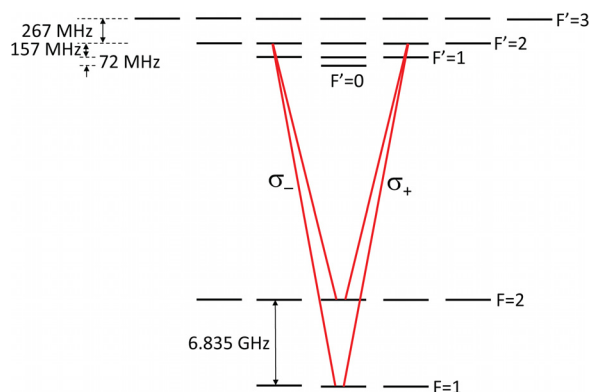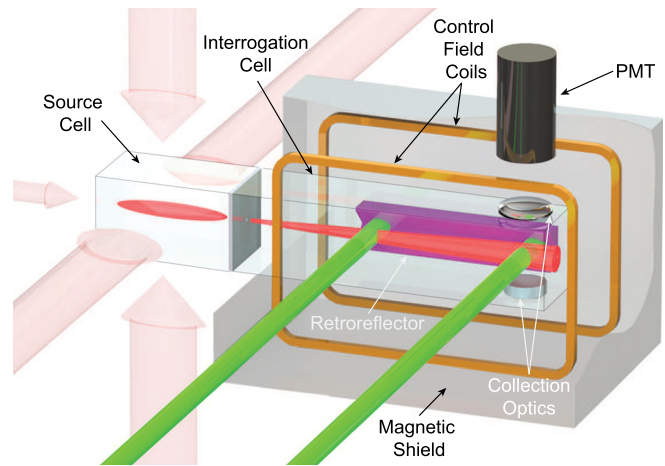

FIG. 3. Schematic of the vacuum system. The Rb^{87} atoms are cooled in a 2D-MOT in the source cell, and the application of the push beam along the longitudinal direction narrows the velocity distribution and improves the beam flux. The atoms travel horizontally into the interrogation cell where they interact with the CPT light ("shown in green") in two zones separated by 4.6 cm. The first zone creates the dark state, and the 2nd zone probes the phase of the atomic coherence by reading out the atoms' state. Above the 2nd CPT zone are collection optics and a photomultiplier tube (PMT) that detects the fluorescent light.

maximize the CPT signal size.[19,20] This retroreflecting optic both converts the polarization of the incident light from σ_+ to σ_- and provides counter propagating light, thereby reducing the impact of the Doppler shift.[12] Ramsey spectroscopy is performed in two CPT zones separated by 4.6 cm within the interrogation cell region of the vacuum system. This length was chosen to meet a short-term instability target of $10^{-11}/\sqrt{\tau}$. The CPT signal is collected using light collection optics and a photomultiplier tube (PMT) placed above the second zone. An aluminum parabolic mirror within the vacuum and below the second CPT zone reflects the fluorescence toward the detection PMT, thus increasing the amount of collected light. A pair of Helmholtz coils outside the vacuum generates a small magnetic field parallel to the propagation direction of the CPT light, necessary to break the degeneracy of the magnetic sublevels of the atoms. The cell and Helmholtz coils are enclosed in a single-layer high-permeability magnetic shield to prevent stray magnetic field gradients from washing out the Ramsey fringe signal. In the current implementation, magnetic field stability is not a limiting factor in the performance of the clock, but in practice, we believe that a two-later magnetic shield will be necessary to achieve reasonable long-term performance in any environment out of the lab.

To characterize the flux and velocity distribution of the cold atomic beam, the fluorescence of the atoms passing through a transverse resonant laser beam is measured using the PMT and analyzed using time-of-flight techniques. The arrival delay of the atom pulse in the second CPT beam is used to estimate the peak velocity of the atom distribution, the shape of the transients in the time-of-flight signal gives access to the width of the velocity distribution, and the size of the fluorescence signal in the steady state allows for an estimate of the atom flux. By tuning the push beam power, the peak velocity of the atomic beam can be changed from ~5 m/s to 20 m/s. This gives the flexibility to fine-tune the Ramsey period of the CPT experiment. However, as the peak velocity of the atoms is changed, the flux of the

FIG. 2. Energy level diagram of the D2 line in ^{87}Rb showing the $\sigma_+ - \sigma_-$ transition used for CPT interrogation.

atoms and the width of the velocity distribution also change. A slower atomic beam typically has a wider velocity distribution, while a faster atomic beam has a narrower distribution. Additionally, the beam flux increases with push beam power up to a point, before falling off.

Another important characteristic of the atomic beam is its physical size. The size of the atomic beam in the interrogation chamber in combination with the flux directly influences the fluorescence signal. Given that the typical divergence of an atomic beam generated from a $2D^+$-MOT is $\sim$30–40 mrad,[17,21–23] the peak velocity of the atomic beam plays a critical role in determining the size of the beam. If the atomic beam is too large (i.e., if the atoms travel too slowly), then the CPT light will be unable to interact with all the atoms and the signal will be reduced. If the beam is smaller (faster atoms), then the light in the second zone will be able to address all the atoms and the signal will be enhanced; however, the Ramsey period will be shorter, and the resulting fringe width will be wider. This trade-off is not obvious and is addressed through experimental optimization. It turns out that the optimal point maximizes the flux and reduces the size of the atomic beam, meaning that the system will likely optimize itself to a peak velocity that is faster than what is described for $2D^+$-MOTs previously.[17] As such, for the data presented below, the signal size was optimized, resulting in a flux of 10^9 atom/s and a peak atomic velocity of $\sim$20 m/s with a longitudinal velocity distribution width of ± 3 m/s, with the resulting Ramsey period of $T_R = 2.3$ ms. For the values chosen for these experiments, the width of the atomic beam is roughly $\sim$1 cm in the second CPT zone, which is larger than the CPT optical beam (5 mm). For comparison, the NIST F7 cesium beam clock has a flux of about 5×10^8 atoms/s, with a mean beam velocity of 230 m/s.[24]

A typical single-zone CPT spectrum, obtained in the pulsed mode by blocking the light in the first CPT zone and measuring the fluorescence from the second zone, is shown in Fig. 4. To obtain the
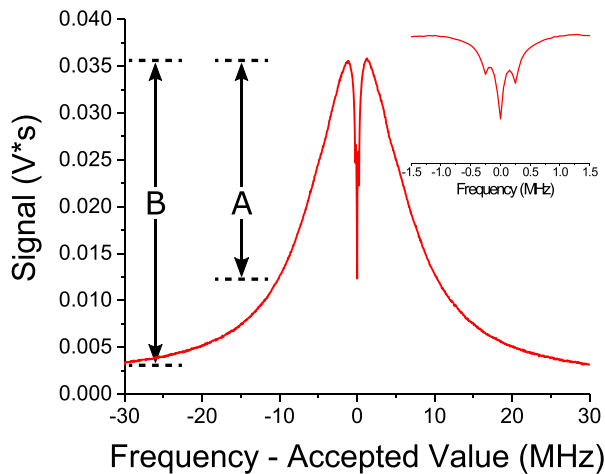
signal, the amplified voltage from the PMT is digitized with a 0.1 ms resolution and integrated over a typical period of 10 ms, while the atom pulse flies through the second CPT zone, thus giving the units of volt second. A contrast ratio (A/B) between the height of the peak (B) and the CPT feature (A) is $\sim$70%; this is comparable to other cold atom CPT systems that use the ^{87}Rb D1 line for interrogation.[14,20] Given this result, we can conclude that the use of cold atoms will eliminate most of the CPT contrast problems existing in thermal vapors interrogated on the D2 line. This is corroborated by the contrast being comparable between D1 and D2 interrogation.[15]

Figure 5 shows Ramsey fringes measured using the apparatus operating in the pulsed mode with no averaging. The fringe spacing is given by the Ramsey period, while the number of fringes is determined by the width of the velocity distribution. The fringe width of $\sim$200 Hz agrees with the measured peak velocity ($\sim$20 m/s) of the atomic beam, and the appearance of more than 14 fringes implies a relatively narrow velocity distribution. The experiment was optimized for short-term stability. While we are able to obtain narrower fringes and higher Q with different parameters, the reduction in the signal-to-noise results in a net decrease in clock performance. In the current implementation, the absolute difference between the clock's center frequency and the accepted value is at most a few Hertz.

An Allan deviation of the frequency instability recorded using an H-maser referenced synthesizer locked to the atomic resonance by alternately probing the sides of the central fringe is shown in Fig. 6. The short-term stability of the clock is typically $3 \times 10^{-11}/\sqrt{\tau}$ and reaches a noise floor of 5×10^{-12}. Analysis of the clock noise shows that the short term is dominated roughly equally by laser frequency noise and laser intensity noise. Other much smaller noise contributions include atom shot noise ($<1 \times 10^{-12}/\sqrt{\tau}$), photon shot noise ($<1 \times 10^{-13}/\sqrt{\tau}$), and local-oscillator noise ($<3 \times 10^{-13}/\sqrt{\tau}$).

Full understanding of the long-term performance of the clock is the subject of on-going work, but there are three significant effects that currently dominate the long-term performance. First, the drift of the clock that limits the long-term stability strongly correlates with the
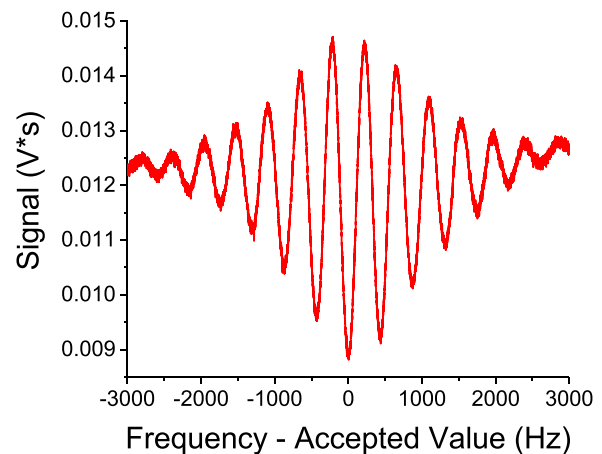
FIG. 4. Single zone CPT fluorescence signal taken in pulsed mode operation with no averaging. The fluorescence contrast, A/B > 70%, shows that nearly complete dark states can be obtained for D2 interrogation through the use of cold atoms as opposed to previously reported low contrasts observed in vapor cells.[15] This measurement was made by holding the carrier frequency of the CPT light locked to the $F = 2 \rightarrow F' = 2$ optical transition, while the EOM modulation frequency is scanned. The inset shows a blowup of the central feature, showing the clock transition surrounded by two magnetically sensitive CPT transitions.

FIG. 5. Ramsey spectrum collected in the pulsed mode, with no averaging. Analysis of the fringes reveals a signal to noise ratio (SNR) in a 1 Hz bandwidth of 140. The magnetically sensitive transitions shown in Fig. 4 are detuned by $\sim$100 fringe envelope linewidths from the $F = 0 \rightarrow F' = 0$ Ramsey spectrum in this plot and play no significant role in distorting or shifting the $F = 0 \rightarrow F' = 0$ resonance.
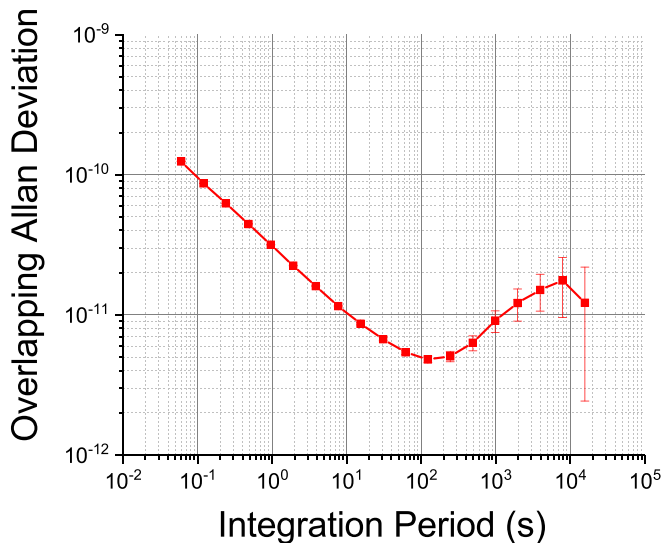
FIG. 6. Frequency stability of the cold atomic beam CPT clock.

drift in the background Rb pressure in both the source and the interrogation cell, which has not been stabilized in the current clock implementation. Second is the end-to-end phase shift: Precise alignment of the optics is needed to match the path length of the two CPT beams, and while any imperfections in this alignment would only impart a fixed frequency offset to the clock output, temperature and environmental instabilities can cause the offset to fluctuate, resulting in long-term instability. By carefully aligning the optical beam paths and by stabilizing the external temperature, we have minimized the instability from the end-to-end phase shift. Given a path length difference of <1 cm between the two CPT arms and periodic lab temperature fluctuations of <1 °C, we estimate an upper bound for the end-to-end phase shifts at the 1×10^{-13} level on time scales of a few hundred seconds, which is lower than the long-term instability that we observe. This effect can be reduced with more careful alignment of the optics. Third is the off-resonant light shifts: as discussed in the beginning of this letter, the use of the D2 line for the CPT interrogation results in larger calculated shifts than for D1 interrogation due to the large number of closely spaced hyper-fine excited states. By measuring the clock frequency vs the laser detuning and modulation index, we have estimated an upper bound on the long-term instability from light shifts of $<1 \times 10^{-12}$. Given the dominant instabilities in the background Rb density and associated frequency instabilities, we have not performed more precise measurements of the light-shift effects thus far.

The combination of a classical thermal-beam atomic clock architecture and cold atoms into a cold beam Ramsey CPT clock is a unique platform for further development of compact atomic-clocks. While the current performance of the clock, short term frequency stability of $3 \times 10^{-11}/\sqrt{\tau}$ averaging down to 5×10^{-12} at 100 s, is not competitive with more well studied vapor-cell clocks, the current results indicate that the clock's performance is limited by the specifics of the experimental implementation, including pressure drifts of the atom source, imperfections in the CPT optical implementation, and technical noise on the lasers, rather than fundamental physics.

REFERENCES

[1] N. F. Ramsey, Phys. Rev. **78**, 695 (1950).
[2] L. S. Cutler, Metrologia **42**, S90 (2005).
[3] E. Arimondo, Prog. Opt. **35**, 257 (1996).
[4] J. Vanier, Appl. Phys. B **81**, 421 (2005).
[5] V. Shah and J. Kitching, Adv. At., Mol., Opt. Phys. **59**, 21 (2010).
[6] P. R. Hemmer, S. Ezekiel, and J. C. C. Leiby, Opt. Lett. **8**, 440 (1983).
[7] A. N. Besedina, V. L. Velichanskiĭ, A. Zibrov, and V. S. Zholnerov, Sov. J. Quantum Electron. **21**, 334 (1991).
[8] J. Robyr, P. Knowles, and A. Weis, IEEE Trans. Ultrason., Ferroelectr., Frequency Control **57**, 613 (2010).
[9] Y. Feng, H. Xue, X. Wang, S. Chen, and Z. Zhou, Appl. Phys. B **118**, 139 (2015).
[10] R. S. B. Pelle, B. Desruelle, and D. Holleville, in 2017 Joint Conference of the European Frequency and Time Forum and IEEE International Frequency Control Symposium (2017), Vol. 479.
[11] C. Xi, Y. Guo-Qing, W. Jin, and Z. Ming-Sheng, Chin. Phys. Lett. **27**, 113201 (2010).
[12] F. X. Esnault, E. Blanshan, E. N. Ivanov, R. E. Scholten, J. Kitching, and E. A. Donley, Phys. Rev. A **88**, 042120 (2013).
[13] E. Blanshan, S. M. Rochester, E. A. Donley, and J. Kitching, Phys. Rev. A **91**, 041401 (2015).
[14] X. Liu, E. Ivanov, V. I. Yudin, J. Kitching, and E. A. Donley, Phys. Rev. Appl. **8**, 054001 (2017).
[15] M. Stähler, R. Wynands, S. Knappe, J. Kitching, A. T. L. Hollberg, and V. Yudin, Opt. Lett. **27**, 1472 (2002).
[16] G. S. Pati, Z. Warren, N. Yu, and M. S. Shahriar, J. Opt. Soc. Am., B **32**, 388 (2015).
[17] K. Dieckmann, R. J. C. Spreeuw, M. Weidemüller, and J. T. M. Walraven, Phys. Rev. A **58**, 3891 (1998).
[18] F. Riehle, P. Gill, F. Arias, and L. Robertsson, Metrologia **55**, 118 (2018).
[19] S. V. Kargapoltsev, J. Kitching, L. Hollberg, A. V. Taichenachev, V. L. Velichansky, and V. I. Yudin, Laser Phys. Lett. **1**, 495 (2004).
[20] X. Liu, V. I. Yudin, A. V. Taichenachev, J. Kitching, and E. A. Donley, Appl. Phys. Lett. **111**, 224102 (2017).
[21] T. Müller, T. Wendrich, M. Gilowski, C. Jentsch, E. M. Rasel, and W. Ertmer, Phys. Rev. A **76**, 063611 (2007).
[22] S. Chaudhuri, S. Roy, and C. S. Unnikrishnan, Phys. Rev. A **74**, 023406 (2006).
[23] N. Castagna, J. Guèna, M. D. Plimmer, and P. Thomann, Eur. Phys. J. Appl. Phys **34**, 21 (2006).
[24] J. H. Shirley, W. D. Lee, and R. E. Drullinger, Metrologia **38**, 427 (2001).